Digest Journal of Nanomaterials and Biostructures Vol. 19, No. 3, July -September 2024, p. 1277 - 1290

Real-time monitoring of nanocellulose suspension concentration using a liquid–solid triboelectric nanogenerator

L. L. Qin[a], Y. Y. Zhou[a], Y. B Lei[a], H. Cai[b], C. Wang[b], W. H. Li[a], Y. L Huang[a], S. D. Qin[a], J. L. Sha[a,*]

[a]*Guangxi Key Laboratory of Clean Pulp & Papermaking and Pollution Control, School of Light Industry and Food Engineering, Guangxi University, Nanning, 530004, China*

[b]*China National Pulp and Paper Research Institute Co., Ltd., Beijing, 100102, China*

Monitoring and controlling the concentration of nanocellulose suspensions is crucial for various industrial processes. Because of the high complexity of traditional concentration measurement devices, new techniques that offer simple, reliable, and real-time concentration monitoring have been developed. Here, we report a method for real-time concentration monitoring using a tubular structured liquid–solid triboelectric nanogenerator (LS-TENG). The LS-TENG was operated in single-electrode mode with a triboelectric layer comprising a polytetrafluoroethylene tube. Further, we systematically investigated the dependence of the device output performance on variables such as concentration, flow rate, tube diameter, and tube material, finding it to be directly proportional to the flow rate and tube diameter and inversely proportional to the concentration. Furthermore, the output current of the LS-TENG exhibited an exponential relationship with the concentration of the nanocellulose suspension and the Reynolds number, achieving a correlation coefficient above 0.94 for the corresponding regression equation. This study provides a direct, accurate, real-time, and self-powered method for monitoring nanocellulose suspension concentrations.

(Received June 24, 2024; Accepted September 3, 2024)

Keywords: Nanocellulose suspension, Triboelectric nanogenerator, Concentration monitoring, Liquid–solid contact electrification, Self-powered sensors

1. Introduction

With advancements in high-performance materials and nanotechnology, nanocellulose has become an increasingly attractive renewable material for advanced applications [1,2]. Nanocellulose has the fundamental properties of cellulose, such as low density, renewability, and biodegradability,

* Corresponding author: shalong910226@hotmail.com

https://doi.org/10.15251/DJNB.2024.193.1277

but also exceptional characteristics such as a large specific surface area, high surface activity and transparency, and favorable hydrophilicity [3-5]. These properties render it ideal for use in food packaging, coatings, fillers for composite materials, and various commercial applications, including water treatment and renewable energy [6-9]. Because the manufacturing and utilization of nanocellulose involve processes where the nanofibrils are in suspension, the accurate monitoring and control of the concentration of nanocellulose suspensions during production is crucial. Currently, there are two main instruments for measuring the concentration of pulp fiber suspensions: blade-type pulp concentration meters and photoelectric concentration meters [10-12]. The blade-type meter quantitatively assesses the concentration based on the frictional force of the blade as the fiber pulp flows past, typically in a pipeline. Its large size makes it suitable for applications with fiber concentrations above 2% [13]. Conversely, a photoelectric concentration meter is generally employed for detecting pulp concentrations below 1%. Photoelectric concentration measuring instruments predominantly exploit the correlation between the light absorption, scattering, and transmission properties of fiber pulp and its concentration [14]. Additionally, ultrasonic concentration detectors determine concentrations based on the capacity of the fiber suspension to absorb and reflect ultrasonic waves [10,15]. Although these instruments can determine fiber suspension concentrations, the measurement devices are typically complex, require stringent installation conditions, and necessitate a continuous external power supply for operation.

Recently, triboelectric nanogenerators (TENGs) have attracted interest in the sensing field because of their straightforward design, cost-effectiveness, and high efficiency [16,17]. Researchers have precisely detected parameters such as vibration, displacement, pressure, flow rate, and concentration by measuring the electrification response of a fluid during liquid contact [18-20]. For example, Zhang et al. proposed a self-powered water-level sensor based on a liquid–solid tubular TENG to measure the draught depth of a sailing ship in real-time [21]. A water-based TENG covered with polycaprolactone-coated fluorinated alumina was designed for wetting monitoring and temperature sensing [22]. To detect the chemical composition and moisture content of liquids, Wang et al. fabricated a liquid–dielectric interface-based TENG with a direct-current output [23]. Chen et al. developed a highly flexible capillary tube TENG as a self-powered active sensor for microliquid biological and chemical sensing applications [24]. That study serves as an important theoretical reference for exploring the liquid–solid contact electrification effect in nanocellulose suspensions and offers a promising approach for the direct, accurate, real-time, and self-powered measurement and control of nanocellulose suspension concentrations.

In this study, a tubular structured liquid–solid TENG (LS-TENG) was designed to investigate its potential for self-powered concentration sensing. The characteristic output signals of the LS-TENG were effectively captured when the nanocellulose suspension flowed through the tube, showing a strong correlation between the output signals and the nanocellulose concentration. By establishing a quantitative relationship between the output signals and the concentration and flow conditions of the nanocellulose suspension, the concentration could be monitored in real-time. This contributes to a better understanding of the interface mechanism of the LS-TENG and provides a straightforward, cost-effective method for detecting nanocellulose suspension concentrations.

2. Materials and methods

2.1. Materials

2,2,6,6-Tetramethylpiperidine-1-oxyl radical-mediated-oxidized cellulose nanofibrils (CNF) and enzymatically hydrolyzed cellulose nanocrystals (CNC) were purchased from Zhongshan Nano Fibers New Materials Co., Ltd. (Guangdong, China). Copper tubes having a thickness of 1 mm were purchased from Xincheng Metal Materials Co., Ltd. (Guangdong, China). Polyvinyl chloride (PVC), polytetrafluoroethylene (PTFE), and silicone tubes having a thickness of 2 mm and inner diameters of 4, 6, and 8 mm were obtained from Gefang Electromechanical Equipment Co., Ltd. (Shanghai, China). Deionized water was obtained from an ultrapure water purification system (Milli-Q, Merck millipore) in the laboratory.

2.2. LS-TENG fabrication

During the material preparation phase, a PTFE tube (40 cm in length) was cleaned with ethanol and deionized water and dried using nitrogen gas to remove any residual electrostatic charge on the tube surfaces. Finally, the Cu tube electrode was affixed to the exit end of the PTFE tube, and external Cu wires were connected to this Cu tube electrode, thus yielding the LS-TENG.

2.3. Measurement

A Cu foil (4×4 cm^2) was fashioned as a collection electrode and suspended inside the beaker to prevent contact between the base of the beaker and the liquid surface. CNF and CNC were uniformly dispersed in deionized water and stirred. The nanocellulose suspension was passed through the LS-TENG using a peristaltic pump (Kamoer, UIP WIFI-S183) and subsequently dropped onto the copper foil collection electrode. The short-circuit current and open-circuit voltage of the LS-TENG were determined using a Keithley 2400 electrometer. The Cu tube and Cu foil collection electrodes of the generator were connected to the positive input terminal of the electrometer to measure the current and voltage, respectively, whereas the negative input terminal of the electrometer was grounded.

2.4. Characterization

The microscopic morphologies of CNF and CNC were examined using transmission electron microscopy (TEM, HT-7700, Hitachi, Japan) at an accelerating voltage of 80 kV. Fourier-transform infrared (FTIR) spectra were recorded using an FTIR spectrometer (TENSOR II, BRUKER, Germany) from 4000 to 400 cm^{-1} to analyze the functional groups of CNF and CNC. X-ray photoelectron spectroscopy (XPS, Thermo Scientific K-Alpha) was employed to determine the chemical composition of CNF and CNC. The conductivity and zeta potential were measured using a conductivity meter (DDS-11A, China) and a nanoparticle size analyzer (Malvern Zeta sizer Nano-ZS90X, UK), respectively.

3. Results and discussion

3.1. Structure and working principle

Fig. 1a shows the basic structure of the LS-TENG, which comprises a PTFE tube and a copper tube electrode. The PTFE tube measured 40 cm in length and had an inner diameter of 4 mm and a wall thickness of 2 mm. A copper electrode was secured to the right end of the tube. Fig. 1b shows the experimental setup of the LS-TENG. Upon activation of the peristaltic pump, the nanocellulose suspension in the beaker was propelled through the tube at a designated flow rate. The working mechanism, based on flow electrification, is presented in Figs. 1c and 1d. A conventional TENG harnesses the triboelectrification effect and electrostatic induction to harvest mechanical energy from the surrounding environment [25]. In a conventional TENG, the electrode is placed behind the triboelectric layer, and output is generated by an electrostatic induction process. In contrast, the LS-TENG in this study is designed to extract energy from the charges in the fluid via flow electrification, thereby generating an induced current [26]. Of note, the electrode is in direct contact with the triboelectric layer, enabling it to collect electricity directly from the suspension, which is energized by friction with the tube, thus minimizing charge loss.

Before the passage of the nanocellulose suspension through the tube, the positive and negative charges in the liquid were balanced, as show in Fig. 1c-i. On contact with the liquid, the inner surface of the PTFE tube becomes negatively charged because of charge affinity. As an electret, PTFE retains this negatively charged layer on its surface for extended periods (Fig. 1c-ii) [25]. As the liquid slides through the tube, an electrical double layer forms, consisting of a Stern layer (a dense layer of charges near the charged surface) and a diffuse layer extending into the liquid. The electrostatic attraction draws the positive charges in the Stern layer toward the negatively charged PTFE surface, whereas the electrostatic repulsion pushes away the negative charges (Fig. 1c-iii) [25,27]. Because the force of electrostatic attraction is significantly stronger than the axial flow force, it is difficult for the positive charges in the Stern layer to migrate upon contact with the copper tube electrode [25]. Consequently, an electrical potential difference forms between the liquid and the copper tube electrodes, and the liquid has a negative potential. Electrons then move from the copper tube electrode to the ground, driven by this potential difference, inducing negative charges (Fig. 1c-iv). Once the imbalanced electrons are discharged, the liquid returns to electrical neutrality (Fig. 1c-v). Because the positive charges in contact with the PTFE surface take longer to flow out than the negative charges, the electrode has an overall positive potential, attracting electrons back to the copper electrode and generating a reverse current (Fig. 1c-vi). This process repeats, resulting in a direct current generated by the LS-TENG (Fig. 1d).

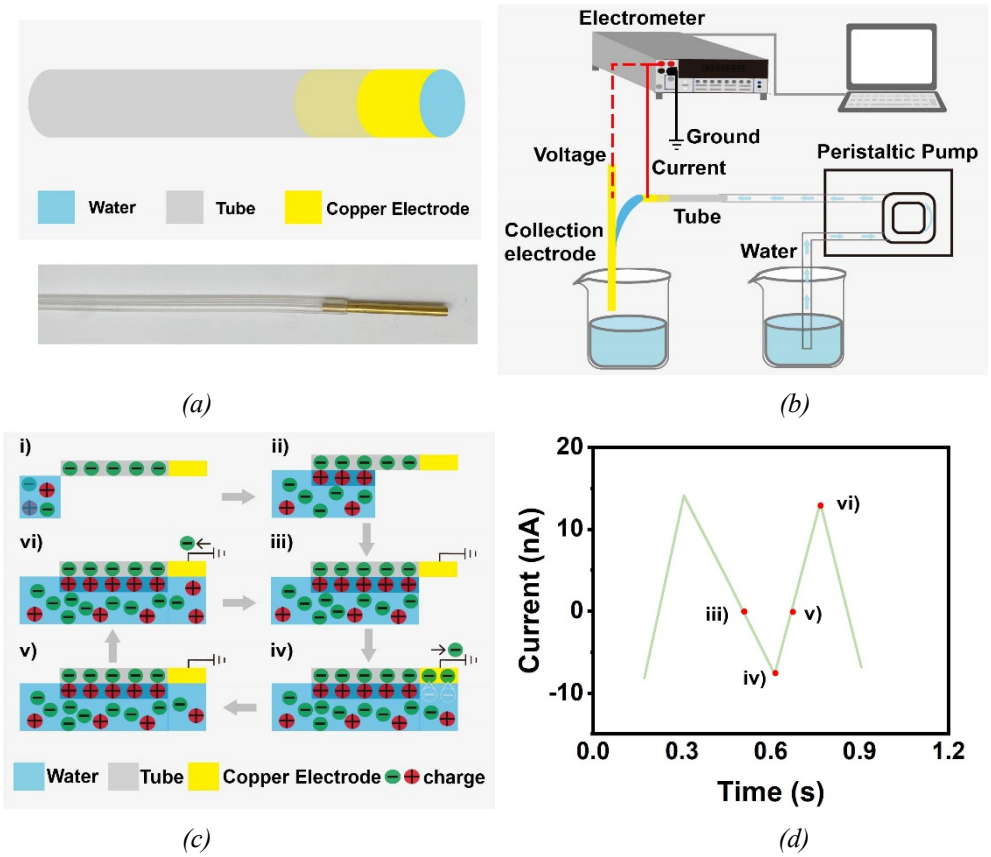

Fig. 1. Structure and working principle. (a) Tubular structure-based single-electrode TENG, (b) test platform, (c) charge transfer process, and (d) short-circuit current of the LS-TENG.

3.2. Characterization of CNF and CNC

TEM micrographs revealed distinct morphologies and sizes for CNF and CNC. CNF displayed a complex, highly entangled, web-like structure, whereas CNC had a simpler, needle-like structure (Figs. 2a and 2b). Length measurements from TEM images (based on the analysis of 100 measurements) showed that CNC had a narrow length distribution, ranging from 200–400 nm and having an average length of 316 nm. In contrast, CNF lengths were more varied, averaging 790 nm, indicating a substantial aspect ratio difference between CNF and CNC. Next, FTIR was used to characterize the functional groups on the CNF and CNC surfaces (Figs. 2e and 2f). Most characteristic for CNF and CNC were similar. The band at approximately 3340 cm^{-1} was attributed to O–H stretching vibrations [28]. In contrast, the bands around 2900 and 1600 cm^{-1} correspond to C–H and C=O stretching vibrations, respectively [29,30]. Finally, the band at 1030 cm^{-1} was assigned to C–O stretching [31]. Further, XPS scans were used to assess the chemical properties of CNF and CNC, and sub-peaks for C–OH and C–OH···O were observed at 533.8 and 531.4 eV, respectively, in the O1s spectra of CNF (Fig. 2g) [32]. Further, in the O1s spectrum of CNC, peaks corresponding to C–OH, C=O, and C–OH···O were observed at 534.1, 532.2, and 530.6 eV, respectively (Fig. 2h) [33]. Therefore, the FTIR and XPS analyses indicate the presence of hydroxyl groups in both CNF and CNC, which can result in a negatively charged cellulose suspension in water. Subsequently, the zeta potential was measured to be -30.47 mV for CNF and -29.40 mV for CNC. The conductivity of the suspension was also measured, revealing an increase in conductivity with the increase in nanocellulose concentration. Specifically, the conductivity of CNF increased from 150 µS/cm at a 0.1% concentration to 500 µS/cm at a 0.4% concentration, whereas CNC conductivity increased from 150 µS/cm to over 600 µS/cm. CNF, which has a larger aspect ratio, exhibited relatively lower conductivities, whereas pelletized CNC, which has a smaller aspect ratio,

had higher conductivity, underscoring the significance of the surface-to-volume ratio in this process (Fig. 2i).

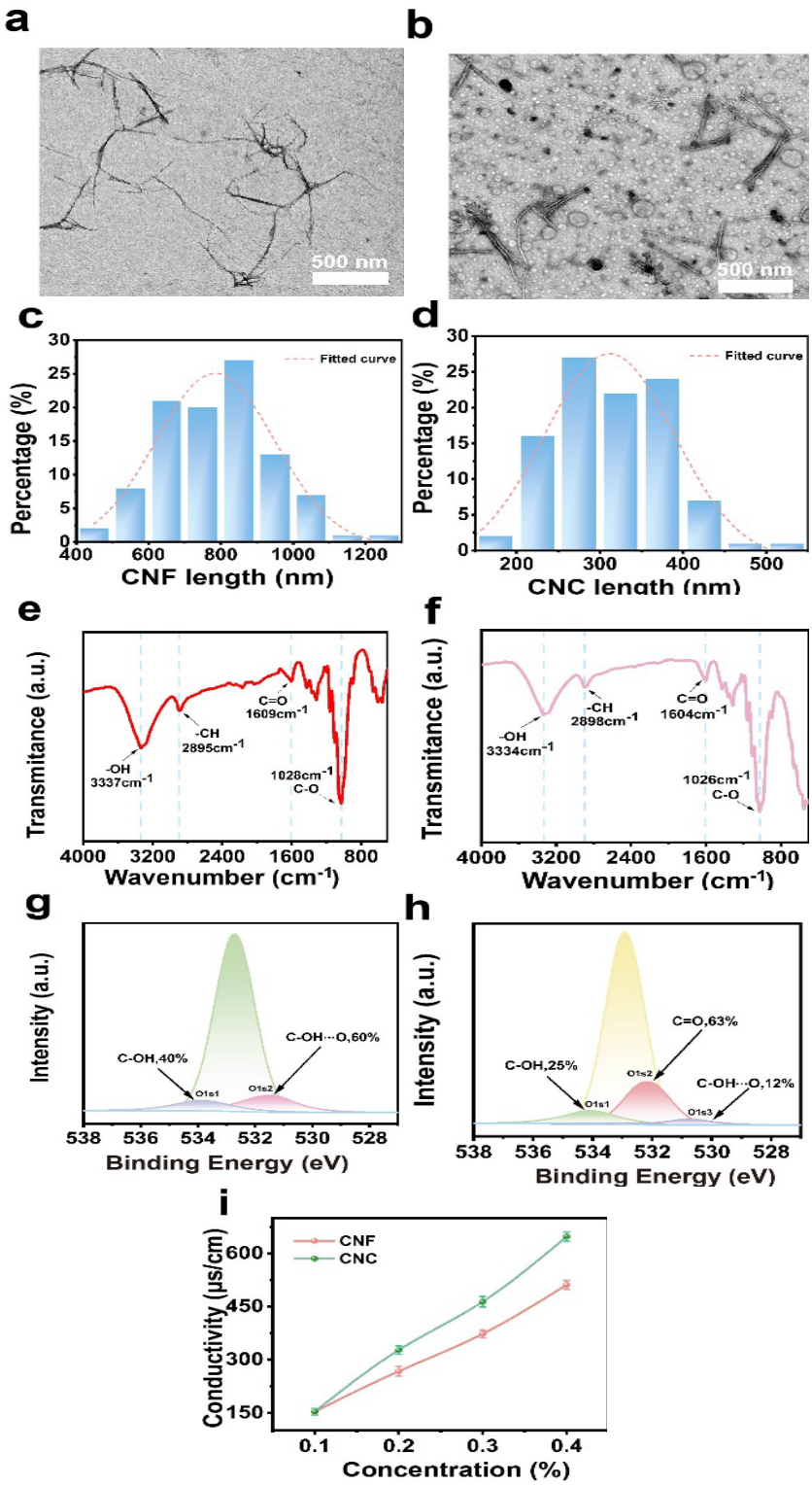

Fig. 2. Characterization of CNF and CNC. TEM images of CNF (a) and CNC (b), length distribution histograms of CNF (c) and CNC (d), surface functional groups analyzed by FT-IR for CNF (e) and CNC (f), XPS analysis of CNF (g) and CNC (h), and conductivity of CNF and CNC (i).

3.3. Output performance of LS-TENG

Electrical signals were generated as the nanocellulose suspension flowed through the LS-TENG. To investigate the correlation between the current and the suspension concentration, experiments were conducted to observe the effects of the concentration, flow rate, tube diameter, and tube material on the output performance of the generator. Fig. 3 shows the changes in output performance with increasing concentration. A PTFE tube was chosen as the triboelectric material for these experiments, and the short-circuit current and open-circuit voltage were recorded at a flow rate of 300 mL/min. Figs. 3a and 3b show the short-circuit current during operation, indicating a negative correlation between current and concentration. As the concentration was increased from 0.1% to 0.4%, the peak current of CNF decreased from 19.1 to 10.5 nA, and that of CNC decreased from 22.1 to 10.8 nA. Figs. 3c and 3d show the open-circuit voltage, which also had an inverse relationship with concentration. Further, the voltage dropped from 3.1 to 1.1 V for CNF and from 3.3 to 1.4 V for CNC with the increase in concentration. This phenomenon can be explained by two factors. First, the FTIR and XPS analyses confirmed the presence of hydroxyl groups in CNF and CNC, resulting in a negatively charged suspension with a negative zeta potential. Thus, an electric double layer formed at the cellulose–water interface, which may hinder the generation of negative charges and impede charge transfer [34,35]. Second, the conductivity of the suspension indicates a direct correlation between the concentration and conductivity (Fig. 2i), suggesting an increase in free ions within the liquid with the decrease in concentration. This increase in free ions weakens electron transfer at the liquid–solid interface, leading to a reduced current signal [34]. However, at the same concentration, CNC demonstrated superior output performance to CNF. This is primarily because of the higher viscosity of CNF compared to CNC [36], which reduces the flowability, thereby restricting solid–liquid interaction and reducing electron transfer.

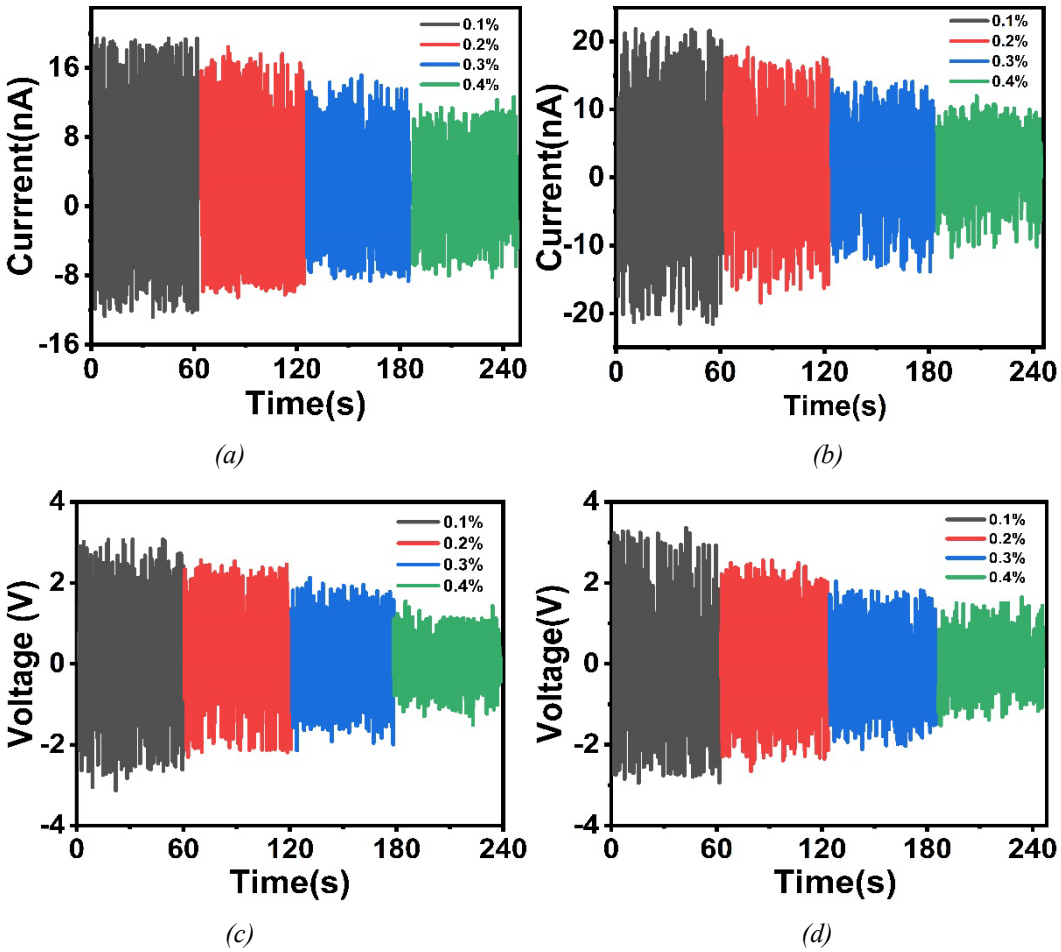

Fig. 3 Effect of concentration on output performance. Short-circuit currents (a, b) and open-circuit voltages (c,d) of CNF (a,c) and CNC (b,d).

Given that flow rate significantly affects the output of the LS-TENG, the flow rate of a 0.1% nanocellulose suspension was varied from 100 to 500 mL/min. Fig. 4 shows the electrical output at these different flow rates, revealing that the flow rate affects the output significantly. The output current of the LS-TENG using CNF as the liquid triboelectric layer increased from 3.5 nA at 100 mL/min to 28.9 nA at 500 mL/min, and the corresponding voltage increased from 1.2 to 4.2 V. When CNC was used as the liquid triboelectric layer, the current increased from 9.5 nA at 100 mL/min to 39.1 nA at 500 mL/min, and the associated voltage increased from 1.6 to 4.3 V. An analysis of fluid motion revealed that an increase in flow rate significantly increases the fluid velocity, leading to more vigorous interactions with the PTFE tube surface. As a result, the frictional interaction between the liquid and solid phases intensifies, enhancing triboelectric charge transfer and notably improving the output performance.

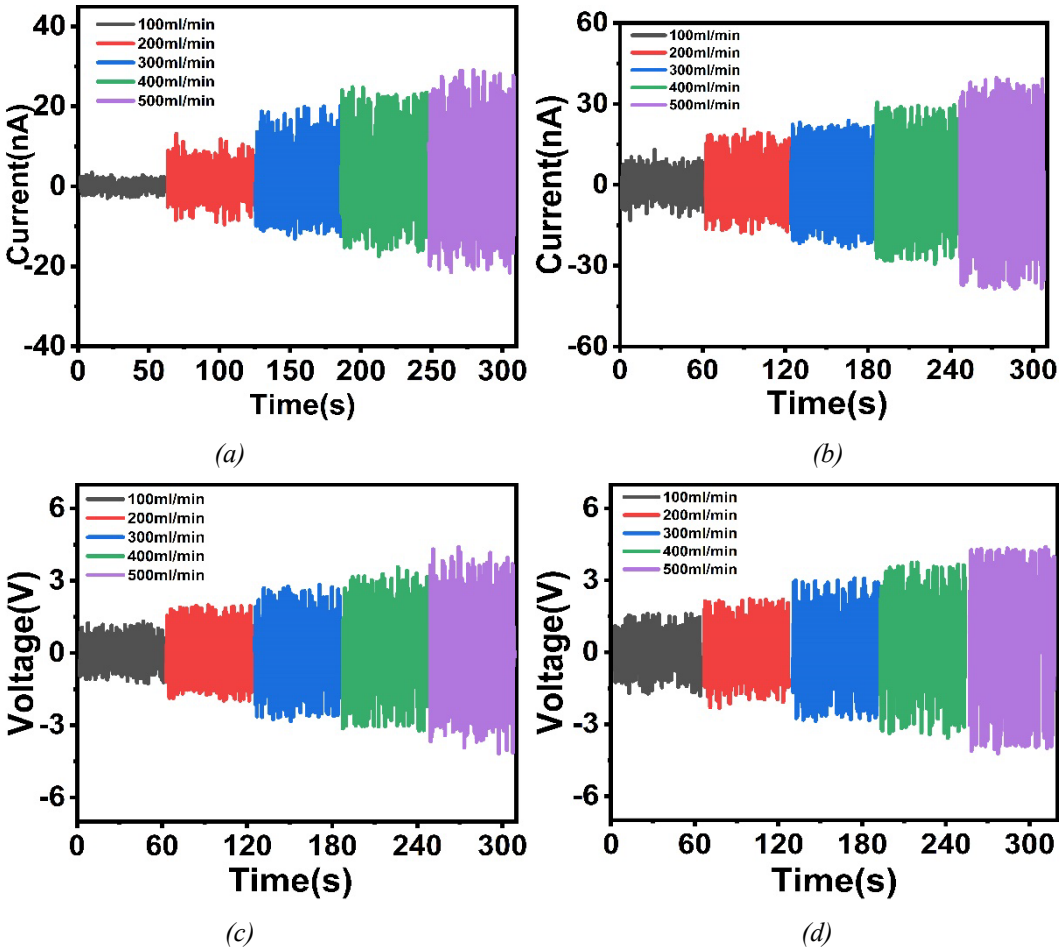

Fig. 4 Effect of flow rate on output performance. Short-circuit currents (a,b) and open-circuit voltages (c,d) of CNF (a,c) and CNC (b,d).

To investigate the effect of the tube diameter, experiments were performed using PTFE tubes having inner diameters of 4, 6, and 8 mm. In these experiments, the short-circuit current was measured with a 0.1% nanocellulose suspension at a steady flow rate of 300 mL/min. As shown in Fig. 5, the short-circuit current progressively increased with the increase in the inner diameter of the tube. This is consistent with the working principle of the device, where a larger tube diameter would increase the effective contact area between the liquid and solid triboelectric layers. Consequently, more fluid interacts with the PTFE tube surface, leading to greater triboelectric charge transfer and an enhanced output current.

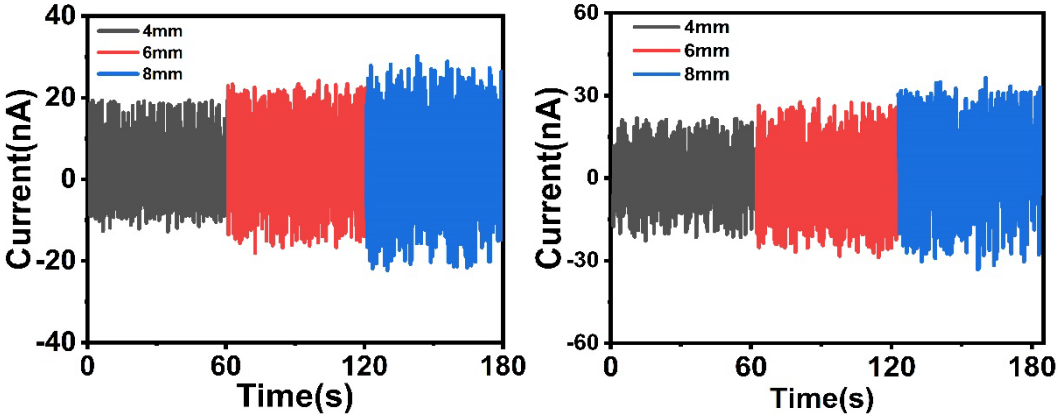

Fig. 5 Effect of tube diameter on the output current for CNF (a) and CNC (b).

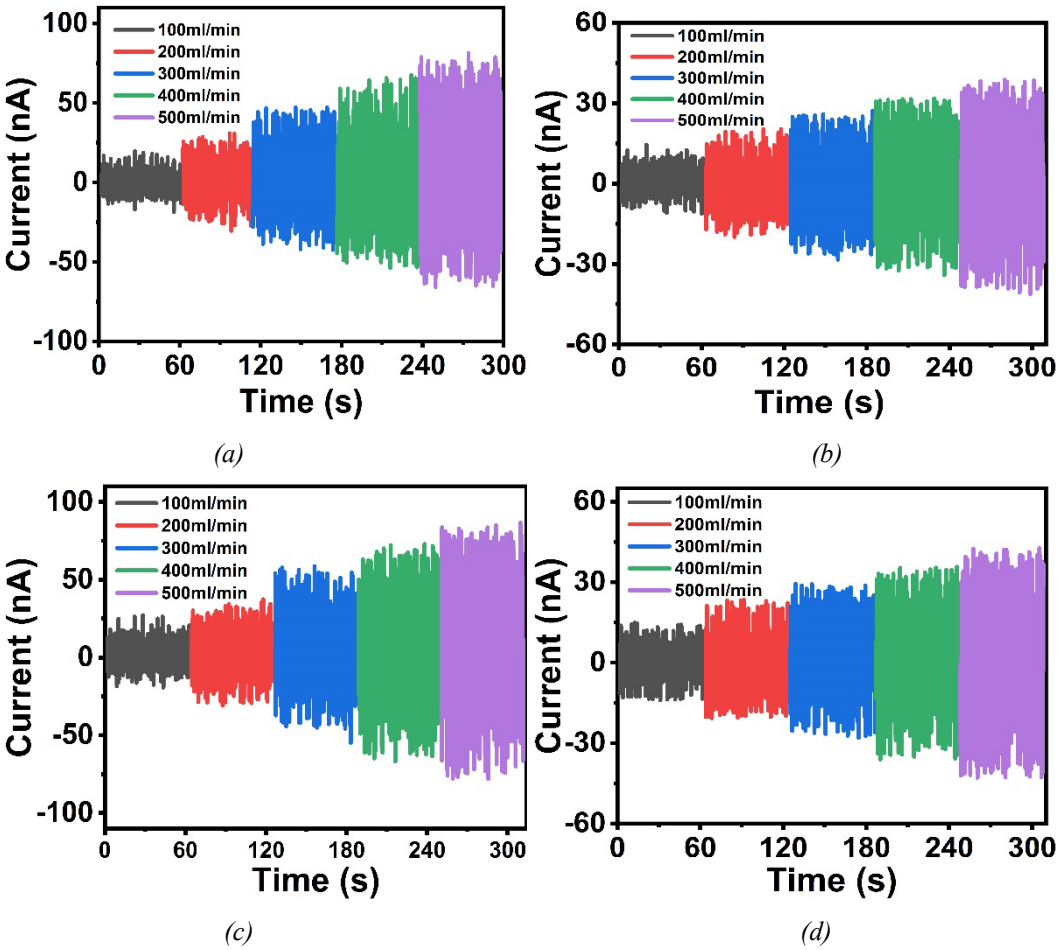

Fig. 6. Effect of tube material on output current. PVC tube with CNF (a) with CNC (b) and silicone tube with CNF (c) and CNC (d).

The choice of solid triboelectric material has a key effect on the output of the LS-TENG because it determines the quantity of transferred triboelectric charge, which is crucial for the output performance of the generator. Therefore, PVC and silicone tubes having inner diameters of 4 mm

were selected as alternative solid triboelectric layers. The output currents were tested individually at flow rates from 100 to 500 mL/min at a 0.1% nanocellulose concentration. Fig. 6 shows the relationship between the current and the tube material. As shown, the output current increased with the increase in flow rate for all materials. For CNF as the liquid triboelectric layer and PVC as the solid triboelectric layer, the output current reached 81.5 nA at a flow rate of 500 mL/min. For the silicone tube, the corresponding current peaked at 85.2 nA. When CNC was used as the liquid triboelectric layer, the currents for PVC and silicone tubes decreased to 38.1 and 42.1 nA, respectively.

Fig. 7 shows a comparison of the recorded currents for LS-TENGs having different tube materials. The highest output current was achieved using a silicone tube, and the current trend across various materials was as follows: silicone > PVC > PTFE. As shown, the output current was significantly affected by the triboelectric series, which ranks materials based on their electron affinity [37]. Materials higher in the series tend to become positively charged upon contact with materials lower in the series, which are negatively charged. The further apart two materials are in the triboelectric series, the more triboelectric charge is generated when the two materials are in contact [38]. Silicone tubes are well-known positive triboelectric materials, whereas PVC and PTFE tubes are negative triboelectric materials. The distance in the triboelectric series between silicone and nanocellulose suspension, which is located between PVC and PTFE in the series, is the greatest, resulting in more intense electron transfer and a higher output current. This rationale also applies to the comparison between PVC and PTFE tubes in contact with nanocellulose suspensions. Under identical conditions, the output current between CNF and either PVC or silicone tubes exceeded that of CNC, whereas the output current between CNF and PTFE was less than that of CNC. This is because CNF is further from the silicone and PVC tubes in the triboelectric series than CNC, leading to greater triboelectric charge transfer. The reverse is true when CNF contacts PTFE.

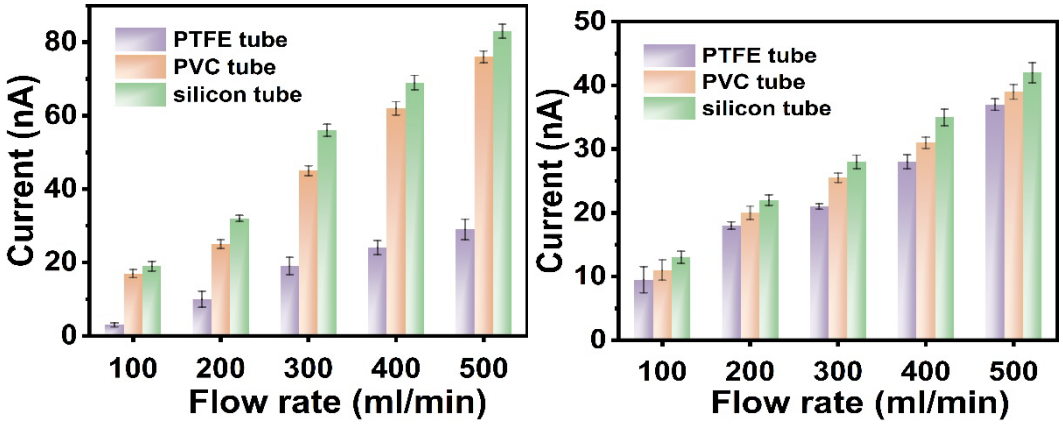

(a) *(b)*

Fig. 7. Effect of tube material on output current. (a) CNF and (b) CNC.

These results indicate that the output characteristics of the LS-TENG are highly sensitive to the concentration and flow rate of the nanocellulose suspension, making it a candidate for real-time concentration monitoring. Consequently, linear regression can be employed to determine the relationships between concentration, flow rate, and current based on the current signal. Figs. 8a and

8b show the output currents at various concentrations in a PTFE tube having an inner diameter of 4 mm. To characterize the fluid flow better, the flow rate was converted to the Reynolds number for water. It was observed that the current output increased with the increase in both concentration and Reynolds number, suggesting a roughly linear relationship within the examined range. However, determining the concentration of nanocellulose suspensions accurately remains challenging when relying solely on the output signals of the LS-TENG. Therefore, to analyze the triboelectric signals and achieve accurate recognition, a regression function was obtained, allowing the conversion of multiple output current values into a probable concentration. Figs. 8c and 8d show the nonlinear regression curves correlating the output current with changes in concentration and the Reynolds number. The regression formula is given by Eq. (1).

$$I = x + y \times exp\left(z \times \frac{\sqrt{c}}{Re}\right) \tag{1}$$

Here, I is the output current, c is the concentration of the nanocellulose suspension, and Re is the Reynolds number. The coefficients are detailed in Table 1. The correlation coefficient for nonlinear regression was greater than 0.94. These results suggest that various concentrations of nanocellulose suspension can be identified from the output electrical signal combined with the nonlinear regression function, thus enabling the identification and determination of nanocellulose suspension concentrations.

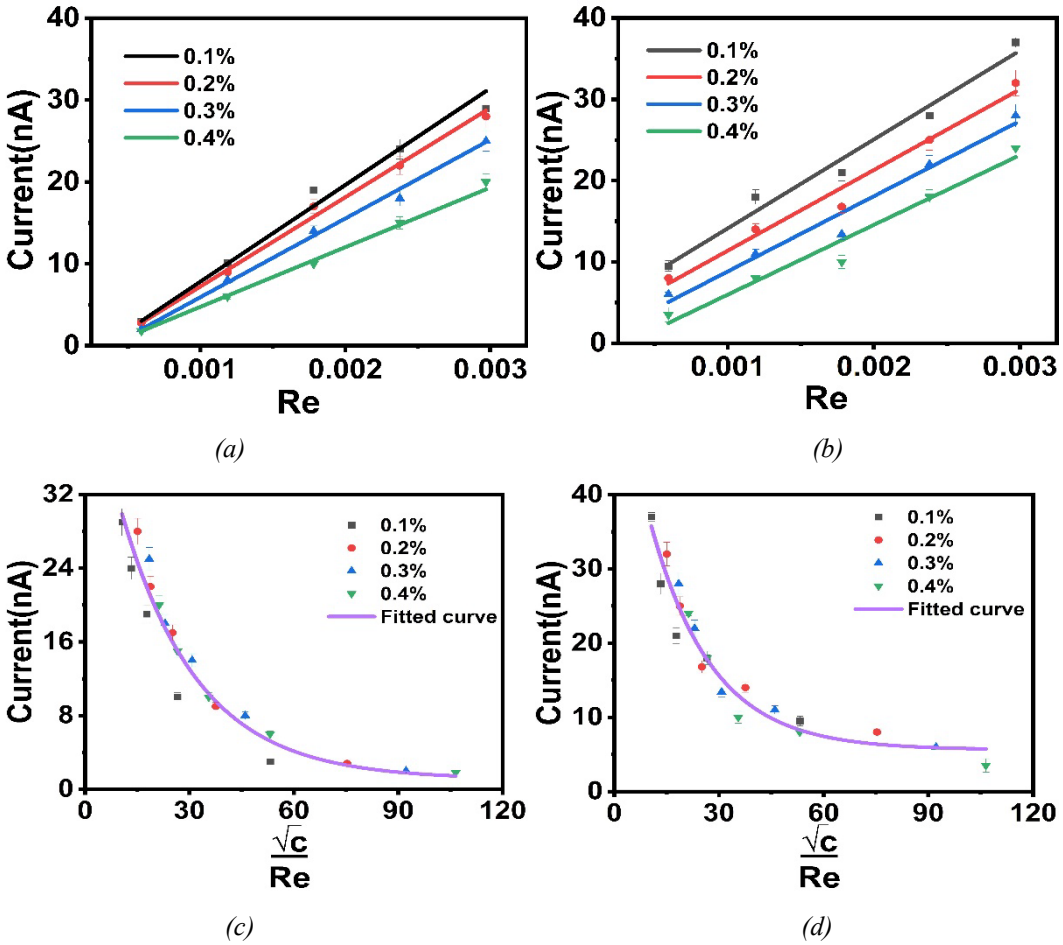

Fig. 8. Regression analysis of output current. (a,b) Linear regression and (c,d) nonlinear regression.

Table 1. Fitting parameters and coefficients of determination of regression equation (Eq. (1)) relating output current and concentration for CNF and CNC.

	x	*y*	*z*	R^2
CNF	1.07	46.76	-0.045	0.95
CNC	5.61	55.22	-0.057	0.94

4. Conclusions

In conclusion, we have designed an LS-TENG having a tubular structure, analyzed the charge generation mechanism at the liquid–solid interface, and examined the effects of concentration, flow rate, tube diameter, and friction materials on the output performance. The output performance was found to be directly proportional to the flow rate and inner tube diameter and inversely proportional to the concentration. Moreover, a strong nonlinear correlation was identified between the concentration and flow rate of the nanocellulose suspension and the output current of the LS-TENG. Further, we have proposed a regression function based on the output current signals. This function achieved a high correlation coefficient of over 0.94, underscoring its potential for broadening the applications of LS-TENGs and determining nanocellulose concentrations.

Acknowledgments

This research was supported by grants from the National Natural Science Foundation of China (22108047), Guangxi Natural Science Foundation of China (2019GXNSFAA185010) and the Foundation of Guangxi Key Laboratory of Clean Pulp & Papermaking and Pollution Control (No.2023GXZZKF72), Guangxi University.

References

[1] L. Chen, S. Y. H. Abdalkarim, H. Yu, X. Chen, D. Tang, Y. Li, K. C. TamNano Research 15(8), 7432 (2022); https://doi.org/10.1007/s12274-022-4374-7

[2] B. Wang, S. Qiu, Z. Chen, Y. Hu, G. Shi, H. Zhuo, H. Zhang, L. Zhong, Carbohydr Polym 299, 120008 (2023); https://doi.org/10.1016/j.carbpol.2022.120008

[3] A. Isogai, Adv Mater 33(28), 2000630 (2021); https://doi.org/10.1002/adma.202000630

[4] O. Nechyporchuk, M. N. Belgacem, J. Bras, Industrial Crops and Products 93, 2 (2016); https://doi.org/10.1016/j.indcrop.2016.02.016

[5] S. Li, and P. S. Lee, Science and Technology of Advanced Materials 18(1), 620 (2017); https://doi.org/10.1080/14686996.2017.1364976

[6] A. Balea, E. Fuente, A. Blanco, C. Negro, Polymers 11, 518 (2019); https://doi.org/10.3390/polym11030518

[7] P. T. Park TaeUng, L. J. Lee JiYoung, J. H. Jo HaeMin, K. K. Kim Kyung Min, Bioresources 13, 7780 (2018); https://doi.org/10.15376/biores.13.4.7780-7791

[8] W. Wu, N. G. Tassi, H. Zhu, Z. Fang, L. Hu, ACS Applied Materials & Interfaces 7(48), 26860 (2015); https://doi.org/10.1021/acsami.5b09249

[9] J. Zhang, J. Fu, X. Song, G. Jiang, H. Zarrin, P. Xu, K. Li, A. Yu, Z. Chen, Advanced Energy Materials 6(14), 1600476 (2016); https://doi.org/10.1002/aenm.201600476

[10] J. Niemi, and T. Löfqvist, Measurement Science and Technology 23(8), 085607 (2012); https://doi.org/10.1088/0957-0233/23/8/085607

[11] C. Zhao, Computer & Digital Engi- neering 40(3), 115 (2012).

[12] Z. Zhao, M. Törmänen, R. Myllylä, Measurement Science and Technology 21(2), 025105 (2010); https://doi.org/10.1088/0957-0233/21/2/025105

[13] E. Engvall, T. Kakuda, Japan Tappi Journal 62(6), 64 (2008); https://doi.org/10.2524/jtappij.62.704

[14] M. Sumida, Proceedings of 2012 International Conference on Fluid Dynamics and Thermodynamics Technologies, IACSIT Press, Singapore, pp.122-128 (2012).

[15] A. C. Belyachits, J. A. Titovitsky, V. M. Serdyuk, International Journal of Innovative Research in Science, Engineering and Technology 3(11), 17101 (2014); https://doi.org/10.15680/IJIRSET.2014.0311001

[16] T. Huang, X. Hao, M. Li, B. He, W. Sun, K. Zhang, L. Liao, Y. Pan, J. Huang, A. Qin, ACS Applied Materials & Interfaces 14(49), 54716 (2022); https://doi.org/10.1021/acsami.2c16271

[17] Y. Zeng, Y. Luo, Y. Lu, X. Cao, Nano Energy 98, 107316 (2022); https://doi.org/10.1016/j.nanoen.2022.107316

[18] H. Cao, Z. Gan, Q. Lv, H. Yan, X. Luo, X. Song, S. Liu, Microsystem Technologies 16(6), 955 (2010); https://doi.org/10.1007/s00542-010-1055-3

[19] S. S. Kwak, S. Lin, J. H. Lee, H. Ryu, T. Y. Kim, H. Zhong, H. Chen, S.-W. Kim, ACS Nano 10(8), 7297 (2016); https://doi.org/10.1021/acsnano.6b03032

[20] H. Zhong, J. Xia, F. Wang, H. Chen, H. Wu, S. Lin, Adv Funct Mater 27(5), 1604226 (2017); https://doi.org/10.1002/adfm.201604226

[21] X. Zhang, M. Yu, Z. Ma, H. Ouyang, Y. Zou, S. L. Zhang, H. Niu, X. Pan, M. Xu, Z. Li, Z. L. Wang, Adv Funct Mater 29(41), 1900327 (2019); https://doi.org/10.1002/adfm.201900327

[22] X. Li, L. Zhang, Y. Feng, Y. Zheng, Z. Wu, X. Zhang, N. Wang, D. Wang, F. Zhou, Adv Funct Mater 31(17), 2010220 (2021); https://doi.org/10.1002/adfm.202010220

[23] J. Wang, Z. Wu, L. Pan, R. Gao, B. Zhang, L. Yang, H. Guo, R. Liao, Z. L. Wang, ACS Nano 13(2), 2587 (2019); https://doi.org/10.1021/acsnano.8b09642

[24] B. D. Chen, W. Tang, C. He, T. Jiang, L. Xu, L. P. Zhu, G. Q. Gu, J. Chen, J. J. Shao, J. J. Luo, Z. L. Wang, Advanced Materials Technologies 3(1), 1700229 (2018); https://doi.org/10.1002/admt.201700229

[25] G. H. Nam, J. H. Ahn, G. H. Lee, C. P. Vo, K. K. Ahn, Advanced Energy and Sustainability Research 1(1), 2000031 (2020); https://doi.org/10.1002/aesr.202000031

[26] B. Ravelo, F. Duval, S. Kane, B. Nsom, J Electrostatics 69(6), 473 (2011); https://doi.org/10.1016/j.elstat.2011.06.004

[27] Z. L. Wang, Rep Prog Phys 84(9), 096502 (2021); https://doi.org/10.1088/1361-6633/ac0a50

[28] L. Bai, N. Bossa, F. Qu, J. Winglee, G. Li, K. Sun, H. Liang, M. R. Wiesner, Environmental Science & Technology 51(1), 253 (2017); https://doi.org/10.1021/acs.est.6b04280

[29] W. H. Danial, Z. Abdul Majid, M. N. Mohd Muhid, S. Triwahyono, M. B. Bakar, Z. Ramli, Carbohydr Polym 118, 165 (2015); https://doi.org/10.1016/j.carbpol.2014.10.072

[30] C. T. Selepe, S. S. Gwebu, T. Matthews, T. A. Mashola, L. L. Sikeyi, M. Zikhali, S. P. Mbokazi, T. S. Makhunga, K. A. Adegoke, N. W. Maxakato, Catalysts 12, 608 (2022); https://doi.org/10.3390/catal12060608

[31] K. Fernández, A. Llanquileo, M. Bustos, V. Aedo, I. Ruiz, S. Carrasco, M. Tapia, M. Pereira, M. F. Meléndrez, C. Aguayo, L. I. Atanase, Polymers 15, 2752(2023); https://doi.org/10.3390/polym15122752

[32] L. Tao, Y. Zheng, Y. Zhang, H. Ma, M. Di, Z. Zheng, RSC Advances 7(43), 27113 (2017); https://doi.org/10.1039/C7RA02716H

[33] T. Javanbakht, W. Raphael, J. R. Tavares, Canadian Journal of Chemical Engineering 94(6), 1135 (2016); https://doi.org/10.1002/cjce.22473

[34] B. Luo, T. Liu, C. Cai, J. Yuan, Y. Liu, C. Gao, X. Meng, J. Wang, S. Zhang, M. Chi, Y. Qin, J. Zhao, X. Zhuang, S. Wang, S. Nie, Nano Energy 113, 108532 (2023); https://doi.org/10.1016/j.nanoen.2023.108532

[35] M.-C. Li, Q. Wu, R. J. Moon, M. A. Hubbe, M. J. Bortner, Adv Mater 33(21), 2006052 (2021); https://doi.org/10.1002/adma.202006052

[36] T. Moberg, K. Sahlin, K. Yao, S. Geng, G. Westman, Q. Zhou, K. Oksman, M. Rigdahl, Cellulose 24(6), 2499 (2017); https://doi.org/10.1007/s10570-017-1283-0

[37] J. F. Hughes, Physics Bulletin 38(11), 424 (1987); https://doi.org/10.1088/0031-9112/38/11/030

[38] C. Li, Y. Qin, H. Zhang, Y. Wang, J. Liao, H. Guo, Nano Energy 120, 109138 (2024); https://doi.org/10.1016/j.nanoen.2023.109138